SUPPLEMENTARY MATERIALS

1.1. Cohort characteristics

The cognitively unimpaired dataset was drawn from five independent cohorts—NACC (n = 2,304), ADNI (n = 348), AIBL (n = 359), CamCAN (n = 623), and HCP-A (n = 721)—and restricted to one scan per participant to minimize data leakage and the risk of overfitting. We first combined these data (n = 4,355; 65.9 ± 13.3 years, 63.2% female) and partitioned them into training (80%, n = 3,484; 65.8 ± 13.5 years, 63.6%), validation (10%, n = 435; 66.3 ± 12.7 years, 61.4% female), and test (10%, n = 436; 66.2 ± 12.9 years, 61.7% female) sets, carefully stratifying by chronological age. **Supplementary Table 1** shows the characteristics of the cognitively unimpaired individuals for training the deep learning model.

Supplementary Table 1. Cognitively unimpaired (CU) dataset characteristics and partitioning for the deep learning model. A total of 4,355 CU participants (aged 23–100 years) from five major cohorts (NACC, HCP, CamCAN, AIBL, ADNI) were split into training (n = 3,484), validation (n = 435), and test (n = 436) sets via age-stratified sampling. Mean age (± SD) and sex distribution (% female) did not differ significantly among the three subsets (ANOVA and χ^2 tests, $p > 0.05$), confirming balanced splits for model development and evaluation.

	Full dataset (n = 4355)	Training (80%, n = 3484)	Validation (10%, n = 435)	Test (10%, n = 436)
Demographics				
Age	65.89 ± 13.33	65.79 ± 13.46	66.35 ± 12.74	66.18 ± 12.88
Sex, F (%)	2752 (63.2%)	2216 (63.6%)	267 (61.4%)	269 (61.7%)

Among all 803 cognitively impaired (CI) individuals with AD/LB pathology, 195 fell into the AD-LB- category, 46 in AD-LB+, 396 in AD+LB-, and 166 in AD+LB+. The AD-LB- subgroup was significantly younger than the three biomarker-positive subgroups (F=4.6, $p < 0.01$), although no significant differences were found among the three biomarker-positive groups themselves. Therefore, in all age-related analyses, chronological age was included as a covariate to control for its potential confounding effects. The proportion of female participants varied among groups, being lowest in AD-LB+ (28.3% *vs*. 39.2-42.4%), and pairwise comparisons showed significant differences between AD-LB+ and each of the other groups (all $p < 0.05$ after multiple test correction). As expected, the highest prevalence of APOE-ε4 carriers appeared in the AD+ groups

(70.5% in AD+LB+ and 65.9% in AD+LB-; $\chi^2 = 386.14$, $p < 0.001$). The cognitively impaired participants spanned mild cognitive impairment (MCI) and dementia, with significantly more individuals manifesting dementia in the AD+ groups.

1.2. Brain age estimation in cognitively unimpaired individuals

We trained a 3D-DenseNet deep learning model to estimate brain age from T1-weighted MRI scans of cognitively unimpaired individuals, encompassing a broad age range (23–100 years), ensuring robust capture of normative aging trajectories.

After training, we evaluated the model on the held out cognitively unimpaired test set (n_{test}=436), which included scans from all five cohorts (n_{NACC}=242, n_{ADNI}=31, n_{AIBL}=38, n_{CamCAN}=67, n_{HCP}=58). This diverse test set assessed the model's ability to generalize across site- and population-level differences. Prior to final performance reporting, we applied a linear bias correction to address a known tendency of brain age estimation models to regress predictions toward the overall mean age of the training set. With bias correction in place, the model achieved an average brain age gap of -0.1 ± 0.22 years and mean absolute error (MAE) of 3.76 ± 0.13 years, a coefficient of determination (R^2) of 0.89, and a Spearman's correlation (r) of 0.93 between predicted and chronological ages. The high R^2 and strong correlation highlight the model's capacity to capture the main trajectory of healthy brain aging across multiple cohorts. Notably, the relatively small average gap (close to zero) after bias correction speaks to the robustness of the model's error distribution.

Next, we applied the model to the longitudinal scans of the cognitively unimpaired individuals in the ADNI dataset. This step was aimed to test the model's reliability in capturing normal aging in the ADNI cohort and to generate a reference point for subsequent comparisons with AD/LB pathology subgroups. After bias correction, the average brain age gap was 0.31 ± 0.11 years and the MAE was 2.26 ± 0.06 years, suggesting robust performance on 691 scans of the cognitively unimpaired data in the ADNI cohort. The overall R^2 was 0.86, with r = 0.93, reaffirming the model's ability to track aging patterns in this population.

1.3. Brain age estimation in pathological groups

Deploying the model trained with normative cohorts, and applying the same bias correction used in cognitively unimpaired participants, we estimated brain age in four cognitively impaired AD/LB pathology subgroups (AD-LB-, AD-LB+, AD+LB-, and AD+LB+). **Figure 3** in the main manuscript shows the distribution of these bias-corrected brain age gaps, and corresponding summary statistics are presented in **Supplementary Table S2**. All AD/LB pathology subgroups showed significantly elevated brain age gaps relative to the cognitively unimpaired reference—indicating

that their structural MRI-derived brain ages exceeded chronological ages to a greater extent than in cognitively unimpaired individuals. Notably, the co-pathology subgroup (AD+LB+) exhibited the largest deviation (6.93 ± 0.29 years; MAE = 7.16 ± 0.27), exceeding that of both AD+LB- (4.64 ± 0.20 years; MAE = 5.85 ± 0.16) and AD-LB+ (2.40 ± 0.55 years; MAE = 4.58 ± 0.37), as well as AD-LB- (2.08 ± 0.26 years; MAE = 4.34 ± 0.17).

Supplementary Table 2. Summary of brain age estimation accuracy and brain age gap across all groups. Shown are the mean absolute error (MAE ± standard error [SE]), and mean bias-corrected brain age gap (BAG ± SE): the cognitively unimpaired (CU) test set, a longitudinal CU subset from ADNI, and four AD/LB pathology subgroups (AD-LB-, AD-LB+, AD+LB-, AD+LB+). While the CU groups exhibit low MAE and near-zero average BAG, all pathological subgroups show significantly elevated BAG, with the AD+LB+ (co-pathology) subgroup displaying the highest deviation (6.93 ± 0.29 years, MAE = 7.16 ± 0.27). These findings suggest a progressive increase in structural "brain aging" when AD and LB pathologies co-occur.

Group	Mean Absolute Error ± SE (years)	Mean Age Gap ± SE (years)
CU Test set	3.76 ± 0.13	-0.10 ± 0.22
CU Longitudinal ADNI	2.26 ± 0.06	0.31 ± 0.11
AD-LB-	4.34 ± 0.17	2.08 ± 0.26
AD-LB+	4.58 ± 0.37	2.40 ± 0.55
AD+LB-	5.85 ± 0.16	4.64 ± 0.20
AD+LB+	7.16 ± 0.27	6.93 ± 0.29

1.4. Interpretability of brain age prediction model

We used gradient-based saliency mapping to identify the brain regions most influencing our 3D-DenseNet model's brain age predictions. Gradients were computed to assess voxel-level sensitivity, with Gaussian smoothing applied to enhance interpretability. Saliency maps were generated for all participants and averaged within each diagnostic group for comparison against cognitively unimpaired individuals to distinguish neurodegeneration-related regions in the AD/LB pathology subgroups. These difference maps revealed that the co-pathology group (AD+LB+) displayed more pronounced saliency among different brain regions, compared to other subgroups. Moreover, comparing co-pathology subgroup with isolated AD pathology subgroup showed heightened saliency near the cholinergic basal forebrain, as well as in parts of the right cingulum. Next, using the Automated Anatomical Labeling (AAL) atlas, we computed the average

saliency values for each brain region to evaluate their relative importance. **Supplementary Tables 3–6** detail the regions exhibiting the highest mean saliency values across the following comparisons: (a) AD+LB+ *vs.* Normal Aging, (b) AD+LB- *vs.* Normal Aging, (c) AD-LB+ *vs.* Normal Aging, and (d) AD-LB- *vs.* Normal Aging.

Supplementary Table 3. **Region-based mean saliency values, using AAL atlas for AD+LB+ *vs.* Normal aging (i.e., CU) comparison.**

Region name	Region number	Mean saliency
Amygdala_R 4202	42	0.012160149
Amygdala_L 4201	41	0.012017412
Hippocampus_R 4102	38	0.011542726
Hippocampus_L 4101	37	0.009637509
ParaHippocampal_R 4112	40	0.006564623
Olfactory_R 2502	22	0.006333057
Cingulum_Ant_R 4002	32	0.006192116
Calcarine_R 5002	44	0.006122886
Olfactory_L 2501	21	0.005885927
Cingulum_Post_R 4022	36	0.005779585
Fusiform_R 5402	56	0.005695175
Thalamus_L 7101	77	0.005512096
Calcarine_L 5001	43	0.005427618
Lingual_L 5021	47	0.005319608
Temporal_Mid_R 8202	86	0.005246252
Cingulum_Mid_R 4012	34	0.005215452
Fusiform_L 5401	55	0.005197588
Occipital_Mid_R 5202	52	0.005189824
Occipital_Inf_R 5302	54	0.004998993
Precuneus_R 6302	68	0.004971811
SupraMarginal_R 6212	64	0.004915192
Lingual_R 5022	48	0.00490186
Cingulum_Post_L 4021	35	0.004890117
Cuneus_R 5012	46	0.004843625
Precuneus_L 6301	67	0.004797317
Temporal_Sup_R 8112	82	0.004726816
Rolandic_Oper_R 2332	18	0.004706172
Occipital_Sup_R 5102	50	0.004692861
Parietal_Inf_L 6201	61	0.004690736
Occipital_Mid_L 5201	51	0.004665844
Angular_R 6222	66	0.004566956
Cuneus_L 5011	45	0.004554632

Temporal_Inf_R 8302	90	0.004438887
Angular_L 6221	65	0.004430278
Temporal_Mid_L 8201	85	0.004420687
Frontal_Med_Orb_L 2611	25	0.004417704
Precentral_R 2002	2	0.004403006
Cingulum_Ant_L 4001	31	0.004296766
Vermis_8 9150	114	0.004196622
Insula_R 3002	30	0.004161854
Cerebelum_9_R 9072	106	0.00413233
Vermis_3 9110	110	0.004097534
Occipital_Sup_L 5101	49	0.004080345
Temporal_Inf_L 8301	89	0.004008973
Cingulum_Mid_L 4011	33	0.003992106

Supplementary Table 4. **Region-based mean saliency values, using AAL atlas for AD+LB- *vs.* CU comparison.**

Region name	**Region number**	**Mean saliency**
Amygdala_L 4201	41	0.010837
Amygdala_R 4202	42	0.0099
Hippocampus_R 4102	38	0.009578
Hippocampus_L 4101	37	0.00789
Cingulum_Post_L 4021	35	0.005151
Lingual_L 5021	47	0.004985
Calcarine_R 5002	44	0.004955
Cingulum_Ant_R 4002	32	0.004788
SupraMarginal_R 6212	64	0.004711
ParaHippocampal_R 4112	40	0.004692
Temporal_Mid_R 8202	86	0.004638
Calcarine_L 5001	43	0.004577
Occipital_Inf_R 5302	54	0.004422
Cingulum_Post_R 4022	36	0.004333
Cuneus_R 5012	46	0.004307
Occipital_Mid_R 5202	52	0.004285
Angular_R 6222	66	0.004232
Fusiform_L 5401	55	0.004228
Olfactory_L 2501	21	0.004204
Thalamus_L 7101	77	0.004153
Fusiform_R 5402	56	0.004144
Temporal_Sup_R 8112	82	0.004054
Cuneus_L 5011	45	0.004038

Olfactory_R 2502	22	0.004025
Lingual_R 5022	48	0.003954

94

95 **Supplementary Table 5**. **Region-based mean saliency values, using AAL atlas for AD-LB+ *vs.* CU**
96 **comparison.**

Region name	**Region number**	**Mean saliency**
Hippocampus_L 4101	37	0.007823
Hippocampus_R 4102	38	0.007373
Amygdala_R 4202	42	0.00612
Amygdala_L 4201	41	0.005658
Vermis_7 9140	113	0.005541
Vermis_6 9130	112	0.005339
Olfactory_L 2501	21	0.004967
Thalamus_L 7101	77	0.004924
Lingual_L 5021	47	0.00473
Calcarine_L 5001	43	0.004576
Calcarine_R 5002	44	0.004511
Temporal_Mid_R 8202	86	0.004503
Cerebelum_6_L 9041	99	0.004395
Cuneus_R 5012	46	0.004281
Vermis_8 9150	114	0.004239
Fusiform_R 5402	56	0.00411
ParaHippocampal_R 4112	40	0.004039
Occipital_Inf_R 5302	54	0.003971
Fusiform_L 5401	55	0.003891
Occipital_Mid_R 5202	52	0.003843
SupraMarginal_R 6212	64	0.003784
Rolandic_Oper_R 2332	18	0.003709
Cerebelum_6_R 9042	100	0.00364
Olfactory_R 2502	22	0.003551
SupraMarginal_L 6211	63	0.003525
Precuneus_R 6302	68	0.003484
Lingual_R 5022	48	0.00343
Cingulum_Post_L 4021	35	0.003239
Temporal_Inf_L 8301	89	0.003101
Precentral_R 2002	2	0.003082
Cerebelum_9_R 9072	106	0.003077
Temporal_Inf_R 8302	90	0.003065
Occipital_Sup_R 5102	50	0.003009

Table S6. **Region-based mean saliency values, using AAL atlas for AD-LB- *vs.* CU comparison.**

Region name	Region number	Mean saliency
Hippocampus_R 4102	38	0.005791
Amygdala_L 4201	41	0.005225
Amygdala_R 4202	42	0.005183
Hippocampus_L 4101	37	0.003883
Lingual_L 5021	47	0.003762
Vermis_8 9150	114	0.00376
Thalamus_L 7101	77	0.003379
Cingulum_Post_R 4022	36	0.003217
SupraMarginal_R 6212	64	0.003167
Temporal_Mid_R 8202	86	0.003085
Calcarine_L 5001	43	0.003053
Rolandic_Oper_R 2332	18	0.003042
Calcarine_R 5002	44	0.003039

1.5. Longitudinal dynamics of brain aging in co-pathology

To further elucidate how LB co-pathology exacerbates AD processes, we evaluated brain aging from a longitudinal perspective. Specifically, we fitted linear mixed models (LMMs) to the 1,574 longitudinal scans from 803 participants across the four AD/LB subgroups, while baseline comparisons were also analyzed via a general linear model, adjusting for baseline age, sex, cognitive state, and level of education, with AD-LB- as the reference group. Model comparisons via Bayesian Information Criterion (BIC) favored a linear model over a quadratic one (ΔBIC = 19.8, where a negative value indicates preference for the quadratic model, and a positive term indicates preference for the linear model).

At baseline, relative to AD-LB-, both AD+LB- ($\beta = 2.25$, SE = 0.46, $p < 0.0001$) and AD+LB+ ($\beta = 3.53$, SE = 0.56, $p < 0.0001$) showed a significantly higher baseline brain age gap, whereas AD-LB+ ($\beta = 0.94$, SE = 0.81, $p > 0.05$) did not differ significantly from AD-LB-. Pairwise contrasts further indicated that AD+LB+ also exceeded AD-LB+ ($\beta = 2.59$, SE = 0.85, $p < 0.01$) and AD+LB- ($\beta = 1.28$, SE = 0.47, $p < 0.01$). Turning to slopes (i.e., the rate of change in brain age gap per year), relative to AD-LB-, which had a negligible yearly slope for brain age gap ($\beta = 0.03$, SE = 0.08, $p > 0.5$), only AD+LB+ and AD+LB- showed significant increases over time. Specifically, AD+LB+ exhibited the steepest rate of change ($\beta = 0.54$, SE = 0.14, $p < 0.001$). AD+LB- also had a significantly higher slope than AD-LB- ($\beta = 0.29$, SE = 0.10, $p < 0.01$), although

this effect was more modest than in the co-pathology condition. In AD-LB+ ($\beta = 0.14$, SE = 0.18, $p > 0.05$), the slope was numerically higher but did not reach statistical significance.

Pairwise contrasts among the pathological subgroups reinforced the heightened vulnerability of AD+LB+. The slope for AD+LB+ was significantly greater than that of AD+LB- ($\beta = 0.25$, SE = 0.06, $p < 0.001$) and AD-LB+ ($\beta = 0.40$, SE = 0.159, $p < 0.01$), underscoring the additional neurodegenerative burden imposed by co-occurring AD and LB pathologies. Overall, these findings indicate that although AD positivity alone accelerates brain aging, the concomitant presence of LB pathology amplifies this effect even further, leading to a more pronounced and rapidly evolving deviation from normative aging trajectories.

1.6. Longitudinal effect of co-pathology on region-specific atrophy

Having established an accelerated overall brain-aging pattern in co-occurring AD and LB pathologies, we next investigated specific neuroanatomical regions to gain a more granular understanding and clarify how these proteinopathies combine to drive atrophy beyond what either pathology alone might incur. Informed by our saliency-map results and prior literature, we focused on the following anatomical targets: (i) the medial temporal lobe (MTL)—aggregating hippocampus, amygdala, entorhinal cortex, and parahippocampal cortex—as these structures are strongly implicated in early AD and exhibited high salience in our interpretability analyses, and (ii) key regions outside the MTL, including the basal ganglia (caudate, putamen, pallidum, accumbens), the middle temporal cortex, and the occipital lobe (lateral occipital, cuneus, pericalcarine, and lingual cortices). In addition to providing more details for each of these regions, we included detailed analyses of the fusiform, cingulum, insula, and MTL sub-regions here. Aligned with our global brain age analyses, BIC comparisons consistently supported linear rather than quadratic trajectories in each region of interest (ΔBIC > 0 for all regions, where a negative value indicates preference for the quadratic model, and a positive term indicates preference for the linear model).

Medial temporal lobe (MTL).

Compared to AD-LB-, both AD+LB- ($\beta = -5.0 \times 10^{-4}$, SE = 1.5×10^{-4}, $p < 0.01$) and AD+LB+ ($\beta = -8.5 \times 10^{-4}$, SE = 1.8×10^{-4}, $p < 0.0001$) exhibited a significantly lower MTL volume at baseline, indicating both pronounced baseline atrophy. In contrast, LB positivity alone (AD-LB+) did not reach statistical significance ($p > 0.05$). Pairwise comparisons also showed that the MTL gray matter volume in AD+LB+ was significantly lower than that of AD+LB- ($\beta = -3.5 \times 10^{-4}$, SE = 1.5×10^{-4}, $p < 0.05$). Although AD+LB- also demonstrated a significant MTL atrophy slope relative to AD-LB- ($\beta = -1.45 \times 10^{-4}$, $p < 0.0001$), the magnitude was smaller than that observed

in the co-pathology condition ($\beta = -2.14 \times 10^{-4}$, $p < 0.0001$). In contrast, LB positivity alone (AD-LB+) did not reach statistical significance at baseline or in the slope. Pairwise post hoc tests confirmed that AD+LB+ outpaced AD+LB- in MTL volume loss ($\beta = -6.90 \times 10^{-5}$, $p < 0.001$), further underscoring a synergistic effect when AD and LB co-occur. Notably, these findings align with the increased saliency observed for medial temporal regions, indicating that co-occurring LB pathology amplifies existing AD-related neurodegeneration within these highly vulnerable limbic areas.

Basal ganglia.

Beyond the MTL, in the basal ganglia, none of the three pathological subgroups differed significantly from AD-LB- at baseline (all $p > 0.05$), and no other pairwise contrasts were significant (all $p > 0.05$). However, in longitudinal trajectories, both AD+LB- ($\beta = -7.3 \times 10^{-5}$, $p < 0.05$) and AD+LB+ ($\beta = -1.21 \times 10^{-4}$, $p < 0.05$) showed significantly faster atrophy relative to AD-LB-, whereas AD-LB+ did not ($p > 0.10$). The co-pathology subgroup (AD+LB+) showed a numerically larger slope β than AD+LB-, though their direct slope comparison failed to reach significance (uncorrected $p = 0.036$, adjusted $p \approx 0.073$), implying a greater vulnerability when both pathologies co-occur. Interestingly, although the fitted trajectories suggest that AD-LB+ volumes are numerically lower than AD+LB- —a pattern not observed in other regions—this difference was not statistically significant ($p > 0.05$).

Occipital lobe.

For the occipital lobe, none of the subgroups differed significantly from AD-LB- at baseline ($p > 0.05$), and pairwise comparisons among them were also nonsignificant ($p > 0.05$). AD+LB+ again showed the largest deviation from AD-LB- in slope ($\beta = -3.27 \times 10^{-4}$, $p < 0.001$), and AD+LB- exhibited a moderate though significant acceleration ($\beta = -2.09 \times 10^{-4}$, $p < 0.001$). LB positivity alone (AD-LB+) did not reach the threshold for significance. Pairwise comparisons revealed that AD+LB+ had a steeper decline than AD+LB- ($p < 0.05$), mirroring findings in the MTL. These results reinforce that concomitant LB pathology intensifies atrophy in visually related cortices beyond what is observed in AD alone.

Middle temporal cortex.

For the middle temporal cortex, AD+LB- ($\beta = -5.0 \times 10^{-4}$, SE = 1.6×10^{-4}, $p < 0.01$) and AD+LB+ ($\beta = -6.6 \times 10^{-4}$, SE = 2.0×10^{-4}, $p < 0.01$) both showed significantly lower baseline volumes than AD-LB-, while AD-LB+ was borderline ($p = 0.06$) and did not reach statistical significance. Pairwise contrasts among AD+LB+, AD+LB-, and AD-LB+ were nonsignificant at baseline (all $p > 0.05$). AD+LB+ displayed a marked β from AD-LB- in slope ($\beta = -3.67 \times 10^{-4}$, $p < 0.0001$), surpassing

the already accelerated rate in AD+LB- ($\beta = -2.04 \times 10^{-4}$, $p < 0.0001$). Although AD-LB+ showed a numerically negative slope, it remained statistically nonsignificant after multiple-test correction. As with other cortical composites, post hoc tests indicated that AD+LB+ declined more quickly than AD+LB- ($p < 0.001$). Notably, AD-LB+ *vs.* AD+LB- also reached significance in slope ($p < 0.01$), and AD-LB+ *vs.* AD+LB+ was significant ($p < 0.0001$), indicating AD+LB+ and AD+LB- each exceed LB alone.

Additional regions assessed included hippocampus, entorhinal cortex, amygdala, fusiform gyrus, cingulum, and insula. The results are presented across the four AD/LB pathological subgroups, offering insights into how co-pathology drives regional atrophy beyond the effects of either pathology alone.

Hippocampus.

At baseline, relative to AD-LB-, AD+LB- ($\beta = -2.37 \times 10^{-4}$, SE = 6.2×10^{-5}, p < 0.001) and AD+LB+ ($\beta = -3.32 \times 10^{-4}$, SE = 7.5×10^{-5}, $p < 0.0001$) each showed significantly lower hippocampal volumes, indicating pronounced baseline atrophy. LB positivity alone (AD-LB+) did not differ significantly from AD-LB- ($p > 0.05$), and pairwise subgroup contrasts among AD-LB+ versus AD+LB- or AD+LB+ were also nonsignificant at baseline. Over time, AD+LB- ($\beta = -4.75 \times 10^{-5}$, $p < 0.001$) and AD+LB+ ($\beta = -7.19 \times 10^{-5}$, $p < 0.0001$) exhibited accelerated atrophy relative to AD-LB-, whereas AD-LB+ again did not reach significance ($p > 0.05$). Pairwise post hoc tests further indicated that AD+LB+ outpaced AD+LB- ($\beta = -2.44 \times 10^{-5}$, SE = 8.0×10^{-6}, $p < 0.01$), underscoring a synergistic effect when LB co-occurs with AD.

Entorhinal Cortex.

At baseline, AD+LB+ ($\beta = -1.89 \times 10^{-4}$, SE = 5.9×10^{-5}, $p < 0.01$) was significantly lower than AD-LB-, while AD+LB- ($\beta = -6.5 \times 10^{-5}$, SE = 4.8×10^{-5}) and AD-LB+ did not differ (both $p > 0.05$). Pairwise contrasts confirmed that AD+LB+ also fell below AD+LB- ($p < 0.05$). Over time, AD+LB- ($\beta = -3.9 \times 10^{-5}$, $p < 0.01$) and AD+LB+ ($\beta = -5.4 \times 10^{-5}$, $p < 0.01$) each displayed faster atrophy than AD-LB-, while AD-LB+ again was not significant ($p > 0.05$). Post hoc tests indicated that AD+LB+ exceeded AD-LB+ in slope ($p < 0.05$), reinforcing an added LB burden in the presence of AD.

Amygdala.

At baseline, AD+LB- ($\beta = -1.33 \times 10^{-4}$, SE = 3.2×10^{-5}, $p < 0.001$) and AD+LB+ ($\beta = -2.20 \times 10^{-4}$, SE = 3.9×10^{-5}, $p < 0.0001$) both showed significantly lower amygdala volumes compared to AD-LB-. Pairwise comparisons further indicated that AD+LB+ was lower than AD-LB+ ($p < 0.05$) and that AD+LB+ also differed significantly from AD+LB- ($p < 0.05$). Longitudinally, AD+LB-

($\beta = -3.4 \times 10^{-5}$, $p < 0.0001$) and AD+LB+ ($\beta = -5.4 \times 10^{-5}$, $p < 0.0001$) declined faster than AD-LB-, whereas AD-LB+ did not differ significantly ($p > 0.05$). Post hoc tests confirmed that AD+LB+ surpassed AD+LB- in its slope ($\beta = -2.1 \times 10^{-5}$, $p < 0.0001$), demonstrating greater atrophy under co-pathology.

Fusiform.

At baseline, none of the subgroups differed significantly from AD-LB- ($p > 0.05$), and no pairwise comparisons reached significance. Over time, AD+LB- ($\beta = -1.68 \times 10^{-4}$, SE = 3.3×10^{-5}, $p < 0.0001$) and AD+LB+ ($\beta = -2.50 \times 10^{-4}$, SE = 4.6×10^{-5}, $p < 0.0001$) each showed accelerated atrophy relative to AD-LB-. LB positivity alone (AD-LB+) did not differ significantly from AD-LB- ($p > 0.05$). Pairwise tests also revealed that AD+LB+ exceeded AD+LB- ($p < 0.01$) and AD-LB+ ($p < 0.001$), mirroring the synergy noted in other regions.

Cingulum.

No baseline differences were found among the groups (all $p > 0.05$). Over time, AD+LB- ($\beta = -8.1 \times 10^{-5}$, SE = 2.4×10^{-5}, $p < 0.01$) and AD+LB+ ($\beta = -1.41 \times 10^{-4}$, SE = 3.4×10^{-5}, $p < 0.001$) both declined faster than AD-LB-. Pairwise contrasts confirmed that AD+LB+ also surpassed AD-LB+ ($p < 0.01$) and AD+LB- ($p < 0.01$), consistent with the co-pathology effect.

Insula.

No subgroup differed from AD-LB- at baseline (all $p > 0.05$). By contrast, over time, AD+LB- ($\beta = -6.5 \times 10^{-5}$, SE = 1.9×10^{-5}, $p < 0.01$) and AD+LB+ ($\beta = -9.6 \times 10^{-5}$, SE = 2.8×10^{-5}, $p < 0.01$) each had a significantly faster slope than AD-LB-, whereas AD-LB+ remained nonsignificant ($p > 0.05$). Pairwise post hoc tests indicated that both AD+LB- and AD+LB+ also exceeded AD-LB+ ($p < 0.05$, $p < 0.01$, respectively). However, AD+LB+ did not differ significantly from AD+LB- ($p > 0.05$).

In sum, these longitudinal volumetric findings demonstrate that LB pathology, when added to an existing AD pathological process, exerts a synergistic effect on neurodegeneration. Whereas isolated LB status often yields borderline or nonsignificant effects, co-pathology (AD+LB+) significantly intensifies atrophy. These results align with our brain-age–based analyses by highlighting the augmented neuroanatomical burden imposed by dual pathology over time.

1.7. Longitudinal effect of co-pathology on cognition

Building on the structural and saliency-map findings, we next examined whether LB co-pathology similarly accelerates longitudinal cognitive decline. To this end, we conducted mixed-effects analyses on two global cognition measures—CDR Sum of Boxes (CDRSB) and the ADAS-Cog

11 (ADAS11)—as well as four domain-specific cognitive composites (memory, language, visuospatial, and executive functioning). To extensively validate the results, additional analyses for Mini-mental state examination (MMSE), modified Preclinical Alzheimer's cognitive composite (PACC) variants, and Functional activities questionnaire (FAQ) are presented subsequently (**Supplementary Figure 1, 2**). Model selection relied on BIC comparisons to determine whether linear or quadratic models best described each cognitive measure.

For CDRSB, a quadratic model was preferred (ΔBIC = −8.78). At baseline, none of the three pathology subgroups (AD+LB-, AD-LB+, AD+LB+) differed significantly from AD-LB- after multiple-comparison correction (all $p > 0.05$). However, over time, the non-linear (Time²) term emerged as the key driver of group differences. Although AD+LB- showed a modestly positive Time² component ($\beta = 0.025$, SE = 0.016, $p > 0.05$), AD+LB+ exhibited a significantly larger acceleration ($\beta = 0.116$, SE = 0.027, $p < 0.0001$) relative to AD-LB-. Pairwise comparisons further revealed that this Time² effect in AD+LB+ significantly exceeded that of AD+LB- ($\beta = 0.091$, $p < 0.001$). A similar pattern emerged for ADAS11, which also favored a quadratic model (ΔBIC = −8.41). At baseline, AD+LB- ($\beta = 1.42$, SE = 0.41, $p < 0.001$) and AD+LB+ ($\beta = 2.73$, SE = 0.55, $p < 0.0001$) both had significantly higher ADAS11 deficits than AD-LB-, and pairwise comparisons indicated that AD+LB+ also exceeded AD-LB+ ($p < 0.01$) and AD+LB- ($p < 0.05$). Over time, while AD+LB- showed a mild positive Time² ($\beta = 0.022$, SE = 0.008, $p < 0.05$), AD+LB+ displayed a more pronounced acceleration ($\beta = 0.54$, SE = 0.14, $p < 0.001$) relative to AD-LB-, and also declined more steeply than AD+LB- ($\beta = 0.32$, $p < 0.01$). These results align with our saliency and volumetric findings showing pronounced medial temporal and subcortical atrophy in AD+LB+ relative to AD+LB-, suggesting that α-synuclein aggregates intensify the atrophic processes already triggered by AD, causing more global clinical severity.

Among the domain-specific composites, we observed a similar pattern of intensified decline in AD+LB+. Based on the BIC values, linear model fits best for the memory (ΔBIC = 0.84) and visuospatial composites (ΔBIC = 19.87), whereas language (ΔBIC = −8.47) and executive function (ΔBIC = −5.54) followed quadratic trajectories. In the memory domain, at baseline, both AD+LB- ($\beta = -0.485$, $p < 0.0001$) and AD+LB+ ($\beta = -0.630$, $p < 0.0001$) were significantly lower than AD-LB-, and additional pairwise tests indicated that AD+LB+ also scored lower than AD+LB- ($p < 0.05$) and AD-LB+ ($p < 0.0001$). Over time, both AD+LB- and AD+LB+ declined significantly faster than AD-LB- ($p < 0.0001$ for each), with AD+LB+ again showing the steepest slope (*vs.* AD+LB-: $\beta = -0.13$, $p < 0.01$). These findings mirror the marked medial temporal lobe atrophy (especially in the hippocampus and entorhinal cortex) observed in our structural analyses. For language, AD+LB- ($\beta = -0.203$, $p < 0.05$) and AD+LB+ ($\beta = -0.294$, $p < 0.01$) were both

significantly worse than AD-LB- at baseline, whereas AD-LB+ was not ($p = 0.576$). No other baseline pairwise contrasts reached significance in language ($p > 0.05$). Over time, both AD+LB- and AD+LB+ exhibited accelerated declines ($p < 0.05$ and < 0.001, respectively), with the strongest acceleration evident in AD+LB+ ($\beta = -0.022$, $p < 0.01$), aligning with the saliency signals in mid-temporal, and fusiform areas. Additionally, AD+LB+ versus AD+LB- in language slope reached significance ($p < 0.05$), confirming a steeper decline under co-pathology. In visuospatial, although baseline differences were less pronounced (i.e., AD+LB- ($\beta = -0.141$, $p > 0.05$) and AD+LB+ ($\beta = -0.227$, $p > 0.05$) were borderline lower than AD-LB-, and no other pairwise tests were significant at baseline), both AD+LB- and AD+LB+ declined faster than AD-LB- ($p < 0.001$, $p < 0.0001$, respectively), with co-pathology showing the steepest slope (β vs. AD+LB- $= -0.16$, $p < 0.001$), consistent with the occipital and mid-temporal saliency increases. A similar pattern emerged for executive function. At baseline, AD+LB- ($\beta = -0.343$, $p < 0.0001$) and AD+LB+ ($\beta = -0.554$, $p < 0.0001$) had a significantly pronounced deficit compared to AD-LB-, and pairwise tests also revealed that AD+LB+ was lower than AD+LB- ($p < 0.05$) and AD-LB+ ($p > 0.05$). Over follow-up, both AD+LB- and AD+LB+ deteriorated faster than AD-LB- (both $p < 0.05$), and AD+LB+ again exceeded AD+LB- ($\beta = -0.005$, $p < 0.05$). These results align with the elevated saliency near the cholinergic nuclei, particularly evident when comparing AD+LB+ to AD+LB-, indicating that LB pathology in the basal forebrain may exacerbate the attentional and executive deficits that already characterize AD.

To further assess the impact of AD and LB co-pathology on cognitive performance, we analyzed longitudinal trajectories for additional cognitive measures not detailed in the main text. Specifically, we examined the MMSE, mPACCdigit, mPACCtrailsB, and FAQ across the four AD/LB pathological subgroups. Using longitudinal mixed-effects models, we explored whether LB co-pathology accelerates cognitive decline in these domains. Model selection was guided by BIC comparisons to identify the best-fitting trajectories (linear or quadratic).

MMSE.

A quadratic model was chosen over linear (ΔBIC $= -10.12$). At baseline, AD+LB- ($\beta = -0.83$, SE $= 0.17$, $p < 0.0001$) and AD+LB+ ($\beta = -1.15$, SE $= 0.21$, $p < 0.0001$) each had lower MMSE scores than AD-LB-, while AD-LB+ did not differ significantly ($p > 0.05$). Over time, AD+LB- ($\beta = -0.08$, SE $= 0.03$, $p < 0.01$) and AD+LB+ ($\beta = -0.22$, SE $= 0.05$, $p < 0.001$) both displayed a significantly larger quadratic decline relative to AD-LB-, with AD+LB+ also surpassing AD+LB- ($\beta = -0.14$, $p < 0.01$).

FAQ.

Model comparisons supported a linear specification over a quadratic one (ΔBIC = 17.64). At baseline, AD+LB- and AD+LB+ each appeared mildly more impaired than AD-LB- (differences ~ 1.25 and 1.47, respectively), although these contrasts were borderline but significant ($p < 0.05$). LB positivity alone (AD-LB+) did not differ significantly ($p > 0.05$). Over time, AD+LB- ($\beta = 1.35$, SE = 0.26, $p < 0.0001$) and AD+LB+ ($\beta = 3.01$, SE = 0.33, $p < 0.0001$) each showed faster decline relative to AD-LB-, and co-pathology (AD+LB+) was the steepest, also exceeding AD+LB- ($\beta = 1.66$, $p < 0.0001$) and AD-LB+ ($\beta = 2.19$, $p < 0.0001$).

mPACCdigit.

A quadratic model offered the best fit (ΔBIC = −32.34). At baseline, AD+LB- ($\beta = -2.62$, SE = 0.32, $p < 0.0001$) and AD+LB+ ($\beta = -3.22$, SE = 0.39, $p < 0.0001$) both scored significantly lower than AD-LB-, while AD-LB+ was borderline ($p > 0.05$). Pairwise tests indicated that AD-LB+ *vs.* AD+LB- ($p < 0.01$) and AD-LB+ *vs.* AD+LB+ ($p < 0.001$) were also significant. Longitudinally, AD+LB- ($\beta = -0.13$, SE = 0.04, $p < 0.01$) and AD+LB+ ($\beta = -0.32$, SE = 0.08, $p < 0.0001$) declined faster than AD-LB-, with AD+LB+ again surpassing AD+LB- ($\beta = -0.19$, $p < 0.01$). These findings align with the effect of co-pathology on memory-related tasks, mirroring hippocampal and entorhinal atrophy patterns.

mPACCtrailsB.

Model selection favored a quadratic approach (ΔBIC = −37.67). At baseline, AD+LB-, AD-LB+, and AD+LB+ each performed worse than AD-LB- ($p < 0.05$, < 0.05, and < 0.0001, respectively), with AD+LB+ showing the largest deficit ($\beta = -3.31$, SE = 0.36). Pairwise contrasts indicated that AD-LB+ was lower than AD+LB- ($p < 0.01$) and AD+LB+ ($p < 0.001$), while AD+LB+ exceeded AD+LB- ($p < 0.05$). Over time, AD+LB- ($\beta = -0.13$, SE = 0.04, $p < 0.01$) and AD+LB+ ($\beta = -0.33$, SE = 0.07, $p < 0.0001$) diverged more rapidly from AD-LB-. The slope for AD+LB+ also surpassed that of AD+LB- ($\beta = -0.20$, $p < 0.01$), paralleling the global trend of increased vulnerability under dual pathology.

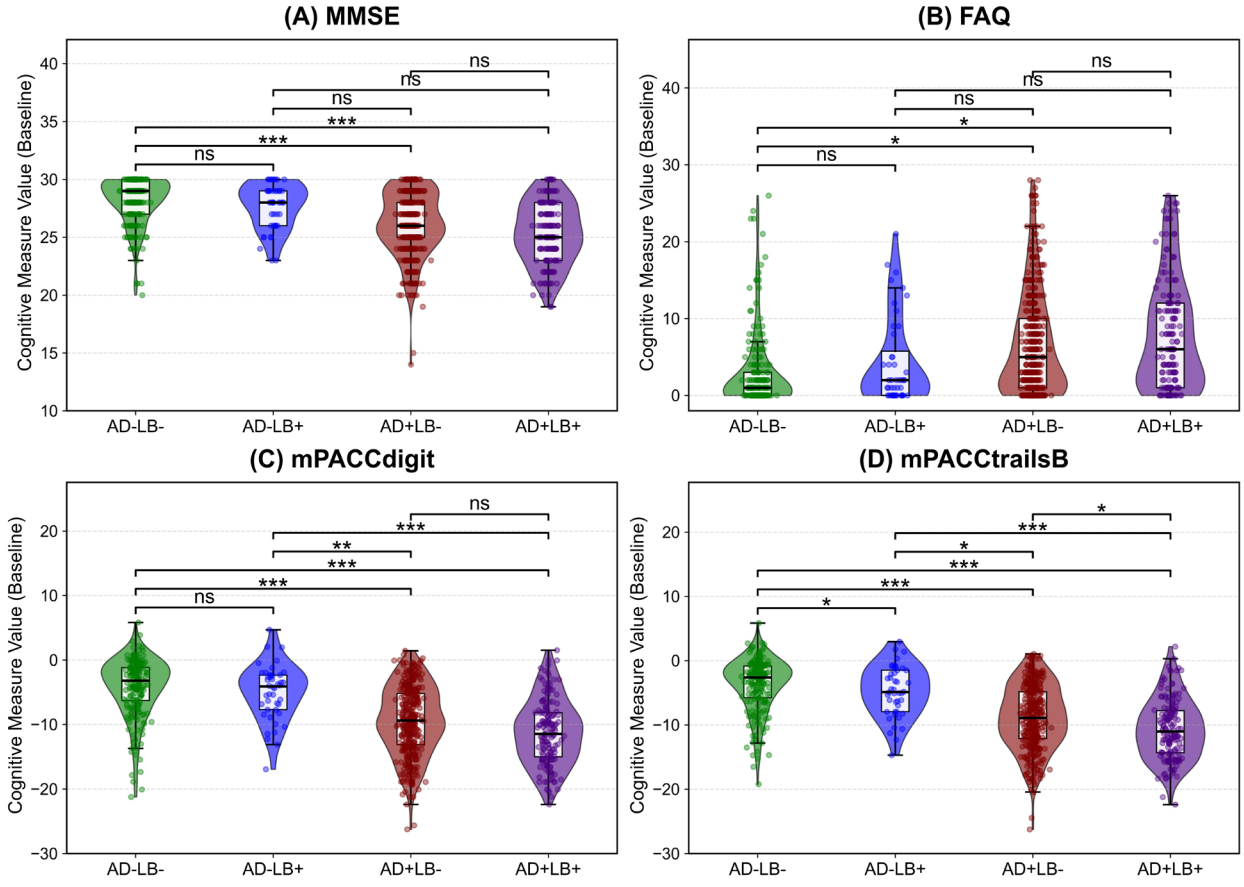

Supplementary Figure 1. Baseline comparisons of additional cognitive measures across AD/LB subgroups. Cognitive measures include **(A)** MMSE, **(B)** FAQ, **(C)** mPACC digit span, and **(D)** mPACC Trails B. Each violin plot depicts the distribution of the cognitive measure at baseline, with boxplots overlaid to illustrate medians and quartiles. The top bars and corresponding significance labels reflect pairwise group comparisons under a generalized linear model adjusted for baseline age, sex, cognitive state, and level of education, with p-values corrected for multiple comparisons (*ns*: not significant; $*p < 0.05$; $**p < 0.01$; $***p < 0.001$).

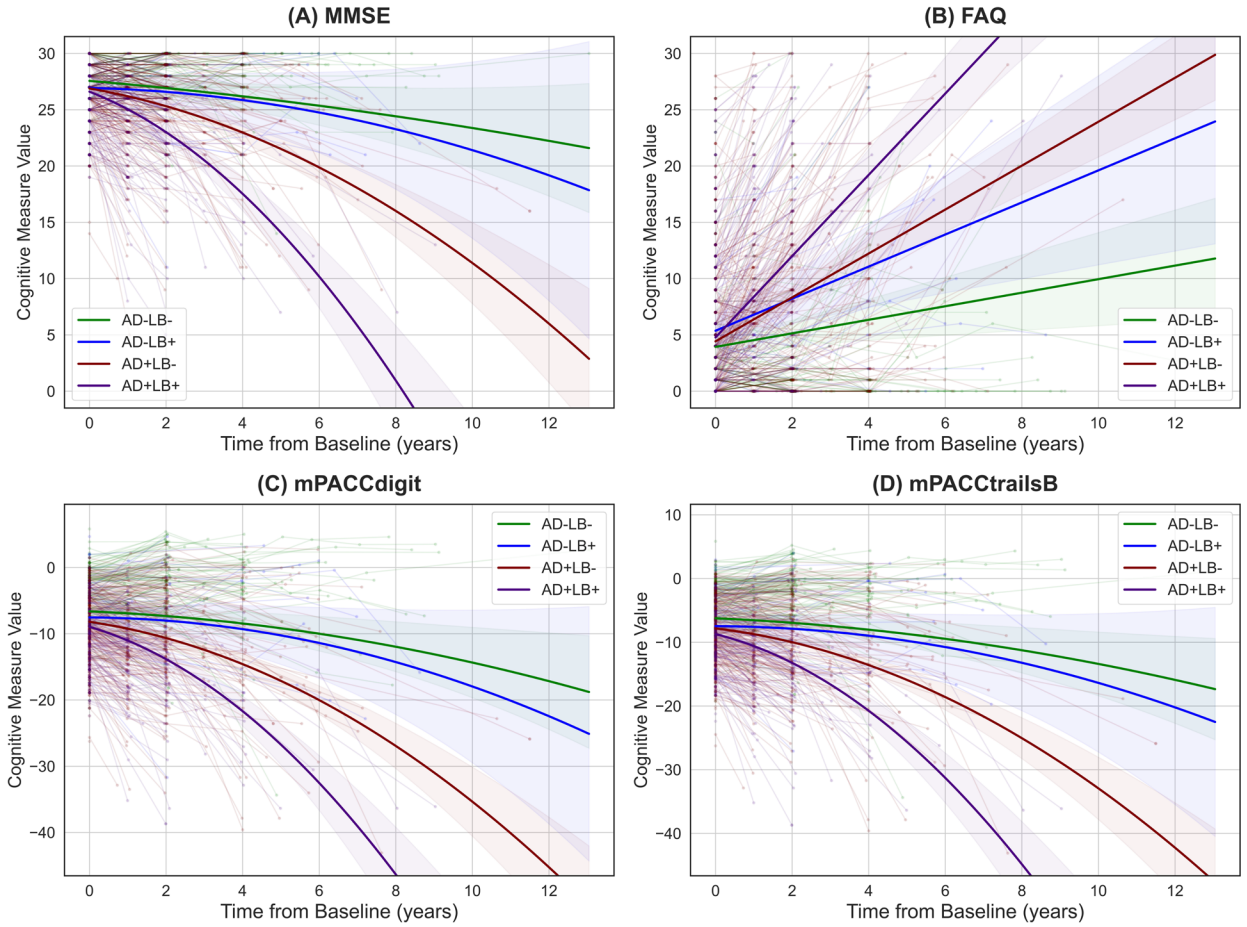

Supplementary Figure 2. **Longitudinal changes in additional cognitive and functional measures.** Each panel shows mixed-effects model fits (thick lines with 95% CI bands) and individual trajectories (thin lines) for **(A)** MMSE, **(B)** FAQ, **(C)** mPACC digit span, and **(D)** mPACC Trails B across the four AD/LB pathological subgroups. Thin lines represent each individual's time course, whereas thicker lines and shaded areas show the estimated trajectories (linear or quadratic trajectories are selected based on the BIC) and corresponding 95% confidence intervals. Notably, the co-pathology subgroup (AD+LB+) exhibits the steepest acceleration or slope of decline in all outcomes. For example, versus AD+LB-, AD+LB+ shows significantly steeper worsening in MMSE ($p < 0.01$), FAQ ($p < 0.0001$), mPACCdigit ($p < 0.01$), and mPACCtrailsB ($p < 0.01$), underscoring that LB co-pathology intensifies AD-related cognitive deterioration. All models are corrected for baseline age, sex, cognitive state, and level of education. Also, all *p*-values are adjusted for multiple comparison.

1.8. Neuropathology results

Leveraging the post-mortem population data ($n = 57$) provided by ADNI, we compared AD-related pathological scores (including Thal, Braak, and CERAD), TDP-43 pathology in the hippocampus and amygdala, and LB pathology evidence (no, brainstem/amygdala predominant, cortical, and olfactory bulb) among the pathology subgroups (**Supplementary Figure 3**). AD+ individuals had higher levels of AD-related pathology, as measured by Thal, Braak, and CERAD scores,

compared to AD- subgroups, which was expected. However, when comparing AD+ individuals with and without LB pathology (AD+LB- *vs.* AD+LB+), no significant differenece was observed. Additionally, there were no noticeable differences in TDP-43 pathology within the hippocampus and amygdala between any of the subgroups. Neuropathological results comparison showed that the obtained results for the co-pathology subgroup are not merely due to more severe AD pathology but are instead driven by the combined effect of co-occurring LB pathology.

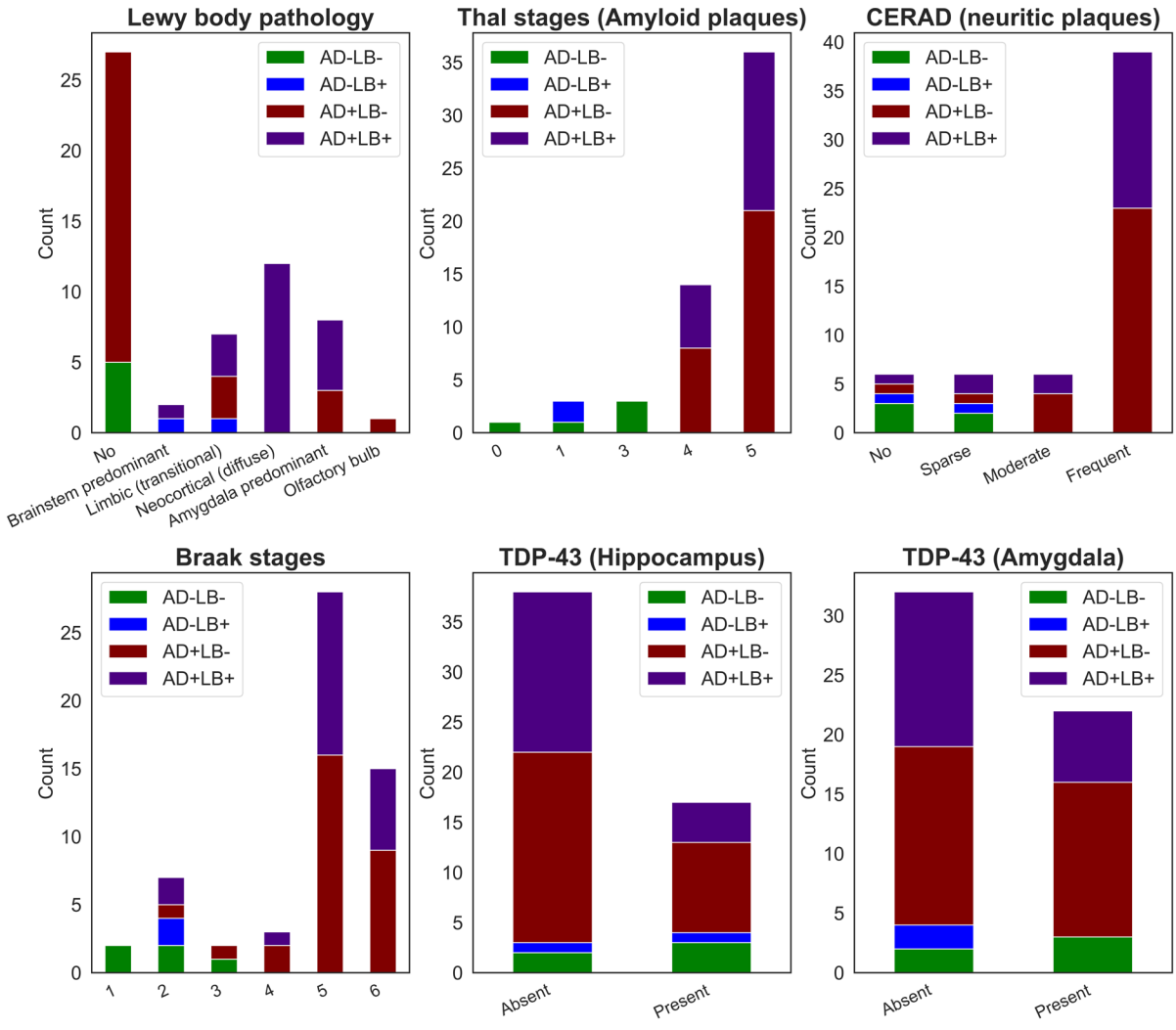

Supplementary Figure 3. **Neuropathology results on the *post-mortem* population data.** Distribution of CSF AD/LB subgroups within the *post-mortem* population data in ADNI, across neuropathological scores, including regional Lewy body pathology, amyloid plaque Thal stages, neuritic plaque CERAD grading, tau Braak stages, and hippocampal and amygdala TDP-43 presence.